

1 **Complement 3a Receptor 1 on Macrophages and Kupffer cells is not required for the**
2 **Pathogenesis of Metabolic Dysfunction-Associated Steatotic Liver Disease**

3
4 Edwin A. Homan¹, Ankit Gilani¹, Alfonso Rubio-Navarro¹, Maya Johnson¹, Eric Cortada¹, Renan
5 Pereira de Lima¹, Lisa Stoll¹, James C. Lo^{1*}.

6
7 **Affiliations:**

8 ¹ Division of Cardiology, Department of Medicine, Cardiovascular Research Institute, Weill
9 Center for Metabolic Health, Weill Cornell Medicine, New York, New York, 10021

10 *Corresponding author. Email: jlo@med.cornell.edu.

11

12

13

14 **Abstract**

15 Together with obesity and type 2 diabetes, metabolic dysfunction-associated steatotic liver
16 disease (MASLD) is a growing global epidemic. Activation of the complement system and
17 infiltration of macrophages has been linked to progression of metabolic liver disease. The role of
18 complement receptors in macrophage activation and recruitment in MASLD remains poorly
19 understood. In human and mouse, *C3AR1* in the liver is expressed primarily in Kupffer cells, but
20 is downregulated in humans with MASLD compared to obese controls. To test the role of
21 complement 3a receptor (C3aR1) on macrophages and liver resident macrophages in MASLD,
22 we generated mice deficient in C3aR1 on all macrophages (C3aR1-M ϕ KO) or specifically in
23 liver Kupffer cells (C3aR1-KpKO) and subjected them to a model of metabolic steatotic liver
24 disease. We show that macrophages account for the vast majority of *C3ar1* expression in the
25 liver. Overall, C3aR1-M ϕ KO and C3aR1-KpKO mice have similar body weight gain without
26 significant alterations in glucose homeostasis, hepatic steatosis and fibrosis, compared to
27 controls on a MASLD-inducing diet. This study demonstrates that C3aR1 deletion in
28 macrophages or Kupffer cells, the predominant liver cell type expressing *C3aR1*, has no
29 significant effect on liver steatosis, inflammation or fibrosis in a dietary MASLD model.

30

31 **Keywords:** obesity, hepatic steatosis, steatohepatitis, C3aR1, macrophage, Kupffer cell

32

33 Introduction

34 Obesity and related metabolic diseases such as type 2 diabetes (T2D) and metabolic
35 dysfunction-associated steatotic liver disease (MASLD) remain a worldwide epidemic with
36 increasing prevalence^{1,2}. MASLD describes the constellation of hepatic lipid deposition,
37 inflammation, and fibrosis associated with obesity and T2D that ultimately leads to MASH
38 cirrhosis, which has become the leading cause of liver transplantation in the United States³⁻⁶.
39 Notably, MASLD is increasingly recognized as an important risk-enhancing factor for
40 atherosclerotic cardiovascular disease^{7,8}.

41 Liver macrophages help to maintain hepatic homeostasis and consist of embryo-derived
42 resident macrophages called Kupffer cells, which self-renew and do not migrate, or peripheral
43 monocyte-derived macrophages, which infiltrate into liver tissue upon metabolic or toxic liver
44 injury and under certain circumstances can take on Kupffer cell-like identity⁹⁻¹³. In obesity, bone
45 marrow-derived myeloid cells migrate to the steatotic liver, and pro-inflammatory recruited
46 macrophages are postulated to drive the progression of MASLD to MASH¹⁴. Spatial
47 proteogenomics reveals a population of lipid-associated macrophages near bile canaliculi that is
48 induced by local lipid exposure and drives fibrosis in steatotic regions of murine and human
49 liver¹⁵. In addition, deep transcriptomic profiling in human MASLD has identified candidate gene
50 signatures for steatohepatitis and fibrosis with possible therapeutic implications¹⁶.

51 Activation of the body's complement system leads to increased cell lysis, phagocytosis,
52 and inflammation¹⁷, and it is increasingly recognized as an important contributor to regulation of
53 metabolic disorders such as T2D and MASLD^{18,19}. In human liver biopsies, higher lobular
54 inflammation scores correlate with activation of the complement alternative pathway²⁰, which
55 can signal *via* the C3a receptor 1 (C3aR1), a G_i-coupled G protein-coupled receptor²¹. The
56 complement 3 polypeptide (C3) is cleaved by C3 convertase to the activated fragment, C3a,
57 which then binds C3aR1²². Complement factor D (CFD), also known as the adipokine adipsin, is
58 the rate-limiting step in the alternative pathway of complement activation^{23,24}.

59 Several studies have reported opposing roles of adiponin and C3aR1 on hepatic steatosis
60 in diet-induced obesity²⁵⁻²⁷. Our lab has found that adiponin/CFD is critical for maintaining
61 pancreatic beta cell mass and function^{28,29}. Murine obese and diabetic models such as *db/db*
62 mice and high fat diet (HFD) feeding result in very low circulating adiponin²³. Replenishing adiponin
63 in *db/db* mice raises levels of C3a and insulin, lowers blood glucose levels, and inhibits hepatic
64 gluconeogenesis²⁸. However, whole-body deletion of C3aR1 decreases macrophage infiltration
65 and activation in adipose tissue, protects from HFD-induced obesity and glucose intolerance,
66 and decreases hepatic steatosis and inflammation³⁰. In a model of fibrosing steatohepatitis,
67 bone marrow-derived macrophages were found to activate hepatic stellate cells, which was
68 blunted in whole-body C3aR1 KO mice³¹.

69 In the present study we aim to explore the macrophage-specific effect of complement
70 receptor signaling in MASLD pathogenesis. To determine the consequences of macrophage and
71 Kupffer cell ablation of C3aR1, we use a murine dietary model of MALFD/MASH, the Gubra
72 Amylin Nash (GAN) diet, which has macronutrient similarities to the Western diet and produces
73 similar histologic and transcriptomic changes to human MASLD/MASH³²⁻³⁴.

74

75 **Results**

76 *C3AR1 is expressed in human and mouse liver, primarily in Kupffer cells.*

77 In the scRNA-Seq database, Human Protein Atlas, *C3AR1* is broadly expressed
78 throughout the body, with increased abundance in tissues rich in immunologic cell types, such
79 as bone marrow and appendix (Fig. 1A)³⁵. In a single-cell transcriptomic database of healthy
80 human liver, *C3AR1* expression predominates in the macrophage and Kupffer cell population,
81 with minimal-to-undetectable *C3AR1* expression in hepatocytes or hepatic stellate cells by
82 scRNA-Seq (Fig. 1B)³⁶. In the mouse liver scRNA-Seq database, Tabula Muris, *C3ar1* is
83 similarly expressed primarily in Kupffer cells (Fig. S1)³⁷.

84

85 *Hepatic CFD and C3AR1 are downregulated in human MASLD/MASH.*

86 We also examined data from Suppli and coworkers, who performed bulk transcriptomic
87 analysis of human liver samples from an age-matched cohort of healthy controls and obese
88 controls without MASLD, as well as MASLD and MASH patients without cirrhosis³⁸. Both *CFD*
89 *and C3AR1* were unchanged in obese subjects without MASLD compared to healthy controls,
90 but both *CFD* and *C3AR1* were significantly downregulated in liver biopsies from both MASLD
91 and MASH patients compared to both healthy controls and obese subjects without MASLD (Fig.
92 1C). Interestingly, both *CFD* and *C3AR1* levels were slightly higher in MASH individuals
93 compared to those with MASLD only.

94

95 *Murine MASH model recapitulates key features of human MASH*

96 At 5 weeks of age, we subjected *C3ar1* flox/flox control mice to standard regular diet
97 (RD) or GAN diet^{32,33}. After 28 weeks of GAN diet, male mice gained body weight compared to
98 RD (Fig. 1D), primarily as fat mass (Fig. S2-3), but weight gain in female GAN-fed mice was
99 attenuated. Histologic signs of MASLD were present in GAN-fed mice (Fig. 1E), most notably
100 hepatic steatosis and hepatocyte ballooning (Fig. 1F), and liver fibrosis measured by collagen
101 deposition nearly doubled with GAN compared to RD (Fig. 1G). Both hepatic *C3ar1* and *Cfd*
102 gene expression were robustly increased on GAN compared to RD, as were markers of
103 macrophage infiltration, hepatic inflammation, and fibrosis, including collagen gene expression,
104 indicating progression to fibrotic MASH (Fig. 1H).

105

106 *Macrophage-specific C3aR1 deletion does not alter glucose homeostasis.*

107 Owing to the differential regulation of the *C3AR1* gene in MASLD between mice and
108 humans, we generated transgenic mice with macrophage-specific deletion of C3aR1 (*C3aR1*-
109 *MφKO*) to target both liver resident macrophages and recruited monocytes. Successful deletion
110 of *C3ar1* in macrophages from the *C3aR1*-*MφKO* mouse was confirmed by quantitative RT-

111 PCR of isolated peritoneal macrophages that were F4/80+ and CD68+ by fluorescence-
112 activated cell sorting (Fig. 2A). In liver tissue, *C3ar1* expression was reduced by ~88% in both
113 male and female C3aR1-M ϕ KO (Fig. 2B). These results indicate that macrophages account for
114 the vast majority of *C3ar1* expression in the liver.

115 When placed on GAN diet, there was no significant difference in weight gain between
116 control and C3aR1-M ϕ KO mice (Fig. 2C). There was similarly no difference in percent lean or
117 fat mass between these mice (Fig. 2D). Glucose tolerance tests performed in fasted mice after
118 27 weeks GAN diet found no significant differences between control and C3aR1-M ϕ KO mice
119 (Fig. 2E). There was also no difference in insulin sensitivity as measured by insulin tolerance
120 tests in male mice (Fig. S4). Insulin resistance as measured by comparing the ratio of fasting
121 glucose level to fasting insulin level (HOMA-IR) was also unchanged between controls and
122 C3aR1-M ϕ KO mice (Fig. S5). Circulating serum ALT levels were unchanged in male control and
123 C3aR1-M ϕ KO mice on GAN diet (Fig. S6).

124

125 *Macrophage-specific C3aR1 deletion does not significantly impact hepatic steatosis or fibrosis.*

126 Liver samples collected after 28-30 weeks of GAN or regular diet did not show significant
127 differences in liver mass between control and C3aR1-M ϕ KO mice (Fig. 2F). Male mice on GAN
128 diet developed similar qualitative appearance on histology (Fig. 2G), and slide image analysis
129 showed similar proportions of lipid droplet area and collagen area (Figs. 2H, 2I). This indicates
130 that there were no significant differences in steatosis or fibrosis between GAN-fed control and
131 C3aR1-M ϕ KO male mice. While *C3ar1* expression was markedly reduced in the C3aR1-M ϕ KO
132 liver tissue (Fig. 2B), there were no detectable gene expression changes in markers of fibrosis,
133 inflammation, or lipid handling (Fig. 2J). Similarly, in female mice there were also no significant
134 differences between control and C3aR1-M ϕ KO mouse liver in a subset of key gene markers of
135 fibrosis or inflammation (Fig. S7).

136

137 *Kupffer cell-specific C3aR1 deletion does not alter weight gain or glucose homeostasis.*

138 To explore whether there may be competing effects between recruited monocytes and
139 liver resident macrophages (Kupffer cells), we next generated Kupffer cell-specific C3aR1
140 knockout mice (C3aR1-KpKO) and fed them GAN diet. Body weight gain was similar between
141 genotypes for both male and female mice (Fig. 3A), and there was no difference in body
142 composition between control and C3aR1-KpKO mice on GAN diet (Fig. 3B). There was similarly
143 no significant difference in glucose homeostasis between the genotypes during a glucose
144 tolerance test (Fig. 3C).

145

146 *Kupffer cell-specific C3aR1 deletion does not significantly impact hepatic steatosis or fibrosis.*

147 Liver mass was not significantly different between control and C3aR1-KpKO mice on
148 GAN diet (Fig. 3D). Liver sections appeared qualitatively similar by histology stained with
149 Masson's trichrome (Fig. 3E). There were similar levels of hepatic steatosis in these mice as
150 measured by percent lipid droplet area (Fig. 3F). When measured by collagen proportional area,
151 there was no significant differences in liver fibrosis between C3aR1-KpKO and control mice
152 (Fig. 3G). While *C3ar1* expression was reduced by 73% in liver tissue of C3aR1-KpKO mice,
153 there were no significant differences in expression of inflammatory, fibrotic, or lipid handling
154 gene markers (Fig. 3H). *C3ar1* expression similarly decreased by ~90% in liver tissue of female
155 C3aR1-KpKO mice fed regular diet compared to control mice (Fig. S8). These data also indicate
156 that Kupffer cells account for ~80% of hepatic *C3ar1* gene expression in our mouse model of
157 MASLD/MASH.

158

159 **Discussion**

160 Overall, we found that macrophage or Kupffer cell expression of *C3ar1* does not impact
161 body weight gain or histologic/transcriptomic features of MASLD/MASH in a murine dietary

162 model. Deletion of C3aR1 in the macrophage population throughout the body, or specifically in
163 Kupffer cells, did not affect weight gain, glucose homeostasis, or extent of hepatic
164 steatosis/fibrosis.

165 Our findings in macrophage-specific C3aR1 KO mice contrast with prior observations in
166 whole-body C3aR1 KO mice³⁰, which are protected from diet-induced obesity, have improved
167 glucose tolerance, and exhibit decreased hepatic steatosis. In both our macrophage- and
168 Kupffer cell-specific C3aR1 KO mice, which had similar degrees of obesity compared to
169 controls, there was no detectable effect on liver steatosis or fibrosis despite the near abrogation
170 of *C3ar1* expression. This raises the possibility that the lower levels of hepatic steatosis and
171 insulin resistance previously observed in the whole body C3aR1 KO mice may be secondary to
172 protection from obesity. Protection from diet-induced obesity in whole-body C3aR1 KO mice
173 may be mediated by a non-macrophage cell type, since our macrophage-specific C3aR1 KO
174 mice were not afforded this protection. The *C3ar1*-expressing cell types that promote obesity
175 and MASLD remains to be determined.

176 Our laboratory recently reported sex-dependent regulation of thermogenic adipose
177 tissue mediated by adipocyte-derived C3aR1³⁹. However, no such sexual dimorphism was
178 observed in hepatic expression of key MASH genes in response to GAN diet in our
179 macrophage- or Kupffer cell-specific C3aR1-deficient mice. Other work has suggested possible
180 compensatory effects from its sister anaphylatoxin receptor C5aR1, with increased cold-induced
181 adipocyte browning and attenuated diet-induced obesity seen in C3aR1/C5aR1 double KO
182 mice⁴⁰.

183 The strengths of our study include careful metabolic and transcriptomic phenotyping of
184 cell type-specific transgenic mice. Some limitations were our use of a single MASLD dietary
185 model and our focus on the C3aR1 pathway. While the GAN diet recapitulates many features of
186 human MASH due to its similarity to Western diet³⁴, relatively low levels of fibrosis were seen in
187 our study, potentially related to initiating the diet at young age; more rapid fibrosis induction has

188 been seen when GAN diet is initiated at older ages⁴¹. Lastly, while *C3AR1/C3ar1* expression is
189 very low in non-macrophage cells (Fig. B, S1), C3aR1 signaling on other hepatic cell types not
190 explored in this study, such as hepatic stellate cells, could mediate the observed effect in the
191 whole-body C3aR1 KO mouse.

192 Deletion of C3aR1 in macrophages generally, or in liver resident macrophages
193 specifically, had no major effect on systemic glucose homeostasis and hepatic steatosis,
194 inflammation, and fibrosis in this murine dietary model of MASLD/MASH. The complement
195 system is a complex entity directing an important part of the body's inflammatory and tissue
196 repair response in MASLD. Further work is needed to elucidate the mechanisms of the role of
197 C3aR1 in the pathogenesis of MASH and cirrhosis.

198

199 **Materials and Methods**

200 *Animals*

201 *C3ar1 flox/flox* mice were on the C57BL/6J background as described⁴². Homozygous
202 LysM-Cre mice on the C57BL/6J background were purchased from Jackson Laboratories
203 (Strain #004781). *C3ar1 flox/flox* homozygous mice were used in the experiments as controls
204 from the same backcross generation³⁹. All mice were maintained in plastic cages under a
205 12h/12h light/dark cycle at constant temperature (22°C) with free access to water and food.
206 Mice were fed regular diet containing 4.5%kcal fat PicoLab Rodent diet 20 (LabDiet) or GAN
207 diet containing 40%kcal HFD (mostly palm oil) with 20% fructose and 2% cholesterol
208 (D09100310, Research Diets) for 28-30 weeks. Fat mass and lean mass were determined via
209 noninvasive 3-in-1 body composition analyzer (EchoMRI). Mice were humanely euthanized with
210 CO₂ inhalation followed by exsanguination by cardiac puncture.

211

212 *Blood chemistry and serum insulin analysis*

213 Mice were fasted overnight (14-16 hours) for glucose tolerance tests and injected
214 intraperitoneally with syringe-filtered D-glucose solution (2g/kg). For insulin tolerance test, mice
215 were fasted for 6 hours and injected with 0.5 mIU/kg insulin. Blood glucose levels were assayed
216 by commercial glucometer (OneTouch) by tail vein blood samples. Plasma insulin levels were
217 measured from mice fasted for 6 hours. Tail vein blood was collected into lithium heparin-coated
218 tubes, centrifuged at 2000xg at 4°C, and plasma insulin levels were determined by ELISA using
219 a standard curve (Merckodia). Serum alanine aminotransferase levels were measured in serum
220 from blood collected via cardiac puncture using a commercially available colorimetric assay
221 (TR71121, ThermoFisher Scientific).

222

223 *Peritoneal macrophage isolation and flow cytometry*

224 Peritoneal macrophages were isolated from as previously described⁴³. Briefly, mice
225 were euthanized then immediately injected intraperitoneally with 10 mL phosphate-buffered
226 saline (PBS, pH 7.4) at room temperature. After a 3-5 minute incubation period, peritoneal fluid
227 was removed with sterile needle and syringe and placed on ice. After centrifugation at 300xg,
228 the pellet was resuspended in PBS containing 2% fetal bovine serum and 0.1% sodium azide.
229 Cells were stained with phycoerythrin-conjugated anti-F4/80 (clone BM8, cat. #123110) and
230 fluorescein isothiocyanate-conjugated anti-CD11b (clone M1/70, cat. #101206) fluorescent
231 antibodies (Biolegend). Stained cells were loaded on MA900 fluorescence-activated cell sorter
232 (Sony), and dual-positive F480+/CD11b+ cells were sorted for subsequent RNA extraction.

233

234 *Histological studies*

235 A mid-distal portion of the left liver lobe was fixed with 10% buffered formalin and
236 transferred to 70% ethanol. Samples were embedded in paraffin, sectioned at ~5µm thickness,
237 and stained with Masson's trichrome. Slides were imaged using Zeiss Axioscan7 at 20x
238 magnification. Histologic analyses were performed using ImageJ software (version 1.53t). Lipid

239 droplet area was quantified by subtracting non-droplet area in the green channel from total
240 section area of 2-3 independent sections. Collagen proportionate area was quantified by
241 measuring total area in the red channel after reducing intensity threshold to 60-70.

242

243 *RNA extraction and real-time quantitative PCR analysis*

244 Total RNA from liver tissue lysates was extracted using Trizol reagent (Invitrogen)
245 followed by RNAeasy Mini kit (Qiagen) as per manufacturer's protocol. RNA was reverse-
246 transcribed using the High Capacity cDNA RT kit (Thermo). Quantitative PCR was performed
247 using SYBR Green Master Mix (Quanta) and specific gene primers on QuantStudio6 Flex Real-
248 Time PCR Systems (Thermo Fisher Scientific) using the delta-delta Ct method. Expression
249 levels were normalized to Ribosomal protein S18 (*Rps18*). Primer sequences are listed in
250 Supplementary Table A.

251

252 *Statistical analyses*

253 All statistical analyses were performed using GraphPad Prism10. Unpaired two-tailed
254 Student's *t* test with Welch correction for most analyses, with Holm-Šídák correction for multiple
255 comparisons where applicable, and $p < 0.05$ was considered statistically significant.

256

257 **Funding**

258 E.A.H. was supported by NIH T32 5T32HL160520-02. A.G. was supported by was
259 supported by ADA 9-22-PDFPM-01. R.P.L was supported by AHA 23DIVSUP1074485. L.S. was
260 supported by AHA 908952 and an Ehrenkranz Young Scientist Award. J.C.L. was supported by
261 NIH R01 DK121140, R01 DK121844, and R01 DK132879. The views expressed in this
262 manuscript are those of the authors and do not necessarily represent the official views of the
263 American Diabetes Association, the American Heart Association, the National Institute of
264 Diabetes and Digestive and Kidney Diseases, or the National Institutes of Health.

265

266 **Acknowledgments**

267 We would like to thank Dr. Baran Ersoy, Dr. Robert Schwartz, and Dr. Saloni Sinha for their
268 technical advice and assistance.

269

270 **Declaration of Competing Interest**

271 None

272

273 **Data Availability**

274 Data will be made available upon reasonable request.

275

276 **Figure Legends**

277

278 **Figure 1. C3AR1 is found in macrophages, is modulated by MASLD/MASH in humans,**
279 **and is induced by a murine dietary model of MASH.**

280 A) Relative *C3AR1* human tissue expression level by tissue, derived from deep sequencing
281 of the mRNA combined dataset (HPA and GTEx) in the Human Protein Atlas, shown as
282 normalized transcripts per million (nTPM). Liver is highlighted in purple and immunologic
283 tissues are highlighted in red.

284 B) Single-cell RNA sequencing distribution of *C3AR1* expression in human liver (tSNE, t-
285 distributed Stochastic Neighbor Embedding).

286 C) Analysis of *CFD* and *C3AR1* expression from liver biopsy samples in patients with
287 MASH, MASLD, obesity without MASLD, and age-matched healthy controls (n = 12-16
288 per group, Welch *t* test with Holm-Šídák correction for multiple comparisons).

289 D) Weight curve in male and female flox/flox control mice placed on GAN high-fat diet
290 compared to regular diet (RD) controls (males, n = 7; females, n = 6).

291 E) Representative liver section staining by Masson's Trichrome in male control mice on RD
292 or GAN diet for 28 weeks (scale bar = 100 μm).

293 F) Lipid droplet area quantification in liver sections from male control mice, excluding
294 vessel lumens (RD, n = 3; GAN, n = 7).

295 G) Collagen area quantification in liver sections of male control mice (RD, n = 3; GAN, n =
296 7).

297 H) Gene expression of key macrophage or fibrosis genes in male control mice on GAN or
298 RD (n = 6 per group).

299 Unpaired two-tailed Student's *t* test (Except 1C as above). Annotations: *, p < 0.05; **, p < 0.01;

300 ***, p < 0.001

301 **Figure 2. C3aR1 deletion in all macrophages does not affect weight gain, glucose**
302 **homeostasis, liver steatosis or fibrosis.**

- 303 A) Expression of *C3ar1* in isolated peritoneal F4/80+/CD68+ cells from flox/flox control mice
304 (n = 6) or C3aR1-M ϕ KO male mice (n = 3).
- 305 B) Expression of *C3ar1* in whole liver from control or C3aR1-M ϕ KO mice (n = 11-12 per
306 male group, n = 13-14 per female group).
- 307 C) Body mass curve of control or C3aR1-M ϕ KO mice on GAN high-fat diet starting at 5
308 weeks of age (n = 11-12 per male group, n = 14 per female group).
- 309 D) Body composition analysis by EchoMRI in control or C3aR1-M ϕ KO mice after 30 weeks
310 GAN diet (n = 6-9 per male group, n = 9-13 per female group).
- 311 E) Glucose tolerance test in control or C3aR1-M ϕ KO mice with 14h fast after 28 weeks
312 GAN diet (n = 6-9 per male group, n = 9-14 per female group).
- 313 F) Liver mass in control or C3aR1-M ϕ KO male mice at time of euthanasia after 30 weeks
314 GAN diet (n = 6-9 per male group, n = 9-14 per female group).
- 315 G) Representative liver section staining by Masson's Trichrome in male control or C3aR1-
316 M ϕ KO mice (scale bar = 100 μ m).
- 317 H) Lipid droplet area in liver sections from male control or C3aR1-M ϕ KO mice, excluding
318 vessel lumens (n = 6-7 per group).
- 319 I) Collagen area in liver sections from male control or C3aR1-M ϕ KO mice (n = 6-7 per
320 group)
- 321 J) Relative fold expression of key gene markers for fibrosis, inflammation, and liver
322 metabolism in whole liver from male control or C3aR1-M ϕ KO mice mice after 30 weeks
323 GAN diet (n = 11-12 per group).

324 Unpaired two-tailed Student's *t* test: Student's *t* test: *, p < 0.05.

325

326 **Figure 3. C3aR1 deletion in Kupffer cells does not affect weight gain, glucose**
327 **homeostasis, liver steatosis or fibrosis.**

- 328 A) Body mass curve on GAN diet in flox/flox control or C3aR1-KpKO mice beginning at 5
329 weeks of age (n = 8-10 per group).
- 330 B) Body composition analysis by EchoMRI in control or C3aR1-KpKO mice after 28 weeks
331 GAN diet (n = 8-10).
- 332 C) Glucose tolerance test in control or C3aR1-KpKO mice with 14h fast after 26 weeks
333 GAN diet (n = 8-10).
- 334 D) Liver mass in control or C3aR1-KpKO male mice at time of euthanasia after 30 weeks
335 GAN diet (n = 8-10).
- 336 E) Representative liver section staining by Masson's Trichrome in control or C3aR1-KpKO
337 male mice (scale bar = 100 μ m).
- 338 F) Lipid droplet area quantified on liver sections of control or C3aR1-KpKO male mice ,
339 excluding vessel lumens (n = 8-9).
- 340 G) Collagen area quantified on whole liver section of control or C3aR1-KpKO male mice (n=
341 8-9).
- 342 H) Relative gene expression in male control or C3aR1-KpKO mice after 30 weeks GAN diet
343 (n = 5-6).

344 Unpaired two-tailed Student's *t* test: **, p < 0.01.

345

346 **Supplementary figures.**

347 S1) Single cell RNA sequencing analysis of *C3ar1* expression in mouse liver tissue (see
348 text).

349 S2) Percent lean and fat mass of flox/flox control mice after 20 weeks of GAN or RD diet (n =
350 6-7 per group).

351 S3) Absolute lean and fat mass of flox/flox control mice after 20 weeks of GAN or RD diet (n
352 = 6-7 per group).

353 S4) Insulin tolerance test in control or C3aR1-M ϕ KO male mice with 14h fast after 29 weeks
354 GAN diet (n = 6-9 per group).

355 S5) HOMA-IR measurement of insulin resistance in control or C3aR1-M ϕ KO mice with 6h
356 fast after 27 weeks GAN diet (n = 6-9 per male group, n = 9-13 per female group).

357 S6) Serum alanine aminotransferase levels in control or C3aR1-M ϕ KO male mice after 30
358 weeks GAN diet (n = 4 per group).

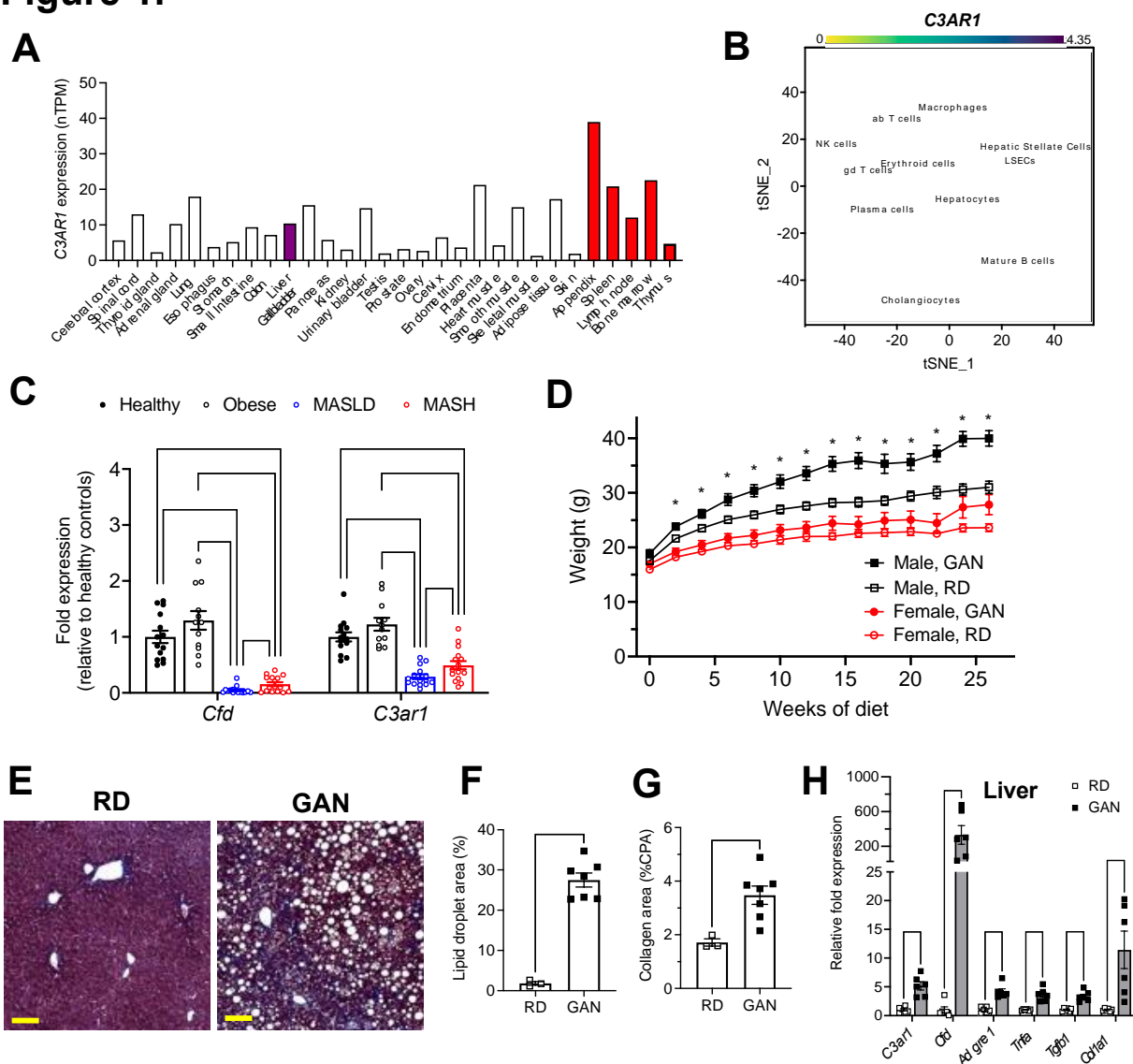
359 S7) Relative gene expression in control or C3aR1-M ϕ KO female mice after 30 weeks GAN
360 diet (n = 13-14 per group).

361 S8) Relative *C3ar1* expression in control or C3aR1-KpKO female mice after 30 weeks RD
362 diet (n = 2-3 per group).

363 Unpaired two-tailed Student's *t* test: **, p < 0.01; ***, p < 0.001.

364

Figure 1.



365

Figure 1. C3AR1 is found in macrophages, is modulated by MASLD/MASH in humans, and is induced by a murine dietary model of MASH.

- A) Relative *C3AR1* human tissue expression level by tissue, derived from deep sequencing of the mRNA combined dataset (HPA and GTEx) in the Human Protein Atlas, shown as normalized transcripts per million (nTPM). Liver is highlighted in purple and immunologic tissues are highlighted in red.
- B) Single-cell RNA sequencing distribution of *C3AR1* expression in human liver (tSNE, t-distributed Stochastic Neighbor Embedding).
- C) Analysis of *CFD* and *C3AR1* expression from liver biopsy samples in patients with MASH, MASLD, obesity without MASLD, and age-matched healthy controls (n = 12-16 per group, Welch *t* test with Holm-Šidák correction for multiple comparisons).
- D) Weight curve in male and female flox/flox control mice placed on GAN high-fat diet compared to regular diet (RD) controls (males, n = 7; females, n = 6).
- E) Representative liver section staining by Masson's Trichrome in male control mice on RD or GAN diet for 28 weeks (scale bar = 100 μ m).
- F) Lipid droplet area quantification in liver sections from male control mice, excluding vessel lumens (RD, n = 3; GAN, n = 7).
- G) Collagen area quantification in liver sections of male control mice (RD, n = 3; GAN, n = 7).
- H) Gene expression of key macrophage or fibrosis genes in male control mice on GAN or RD (n = 6 per group). Unpaired two-tailed Student's *t* test (Except 1C as above). Annotations: *, p < 0.05; **, p < 0.01; ***, p < 0.001.

366
367

Figure 2.

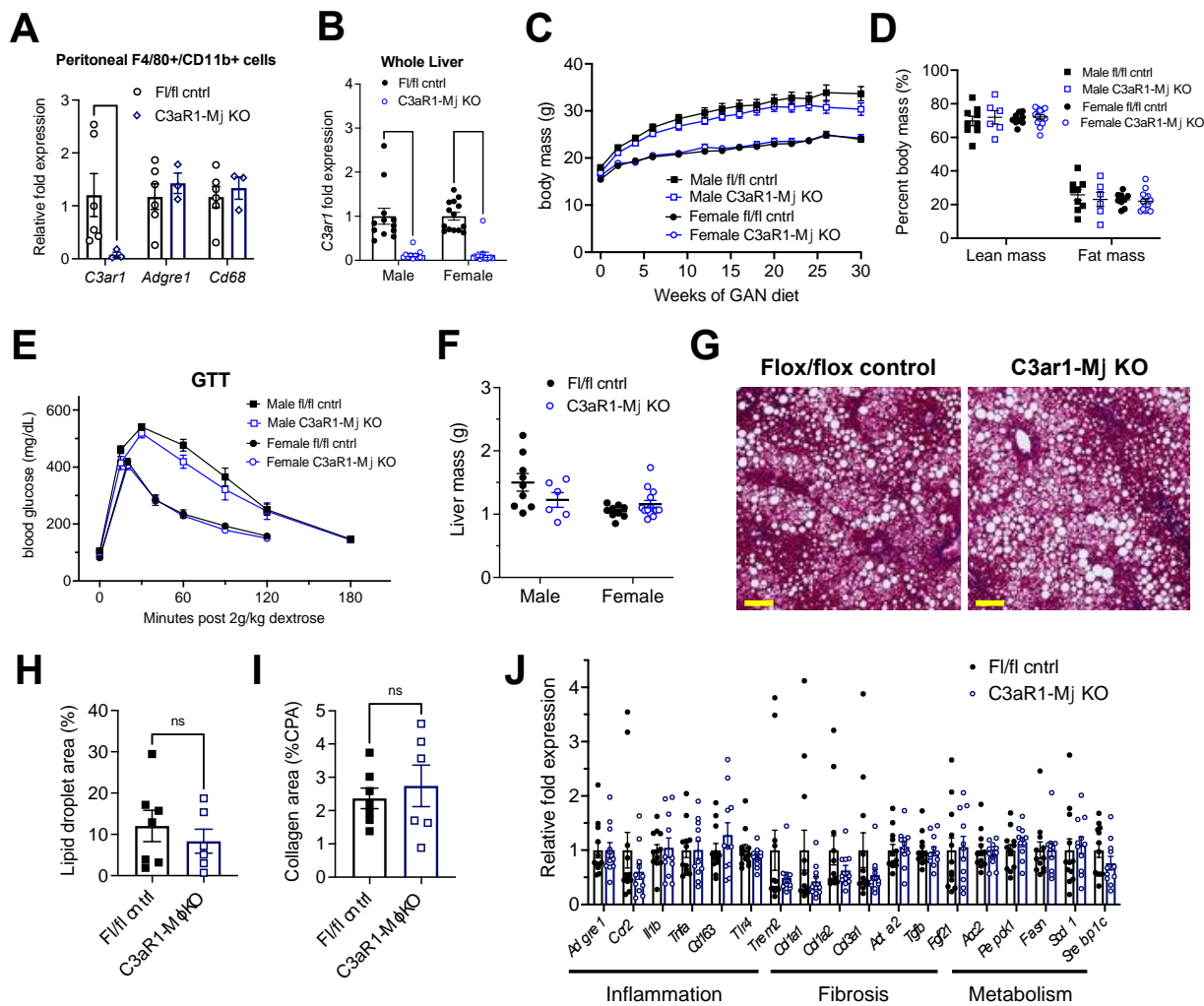


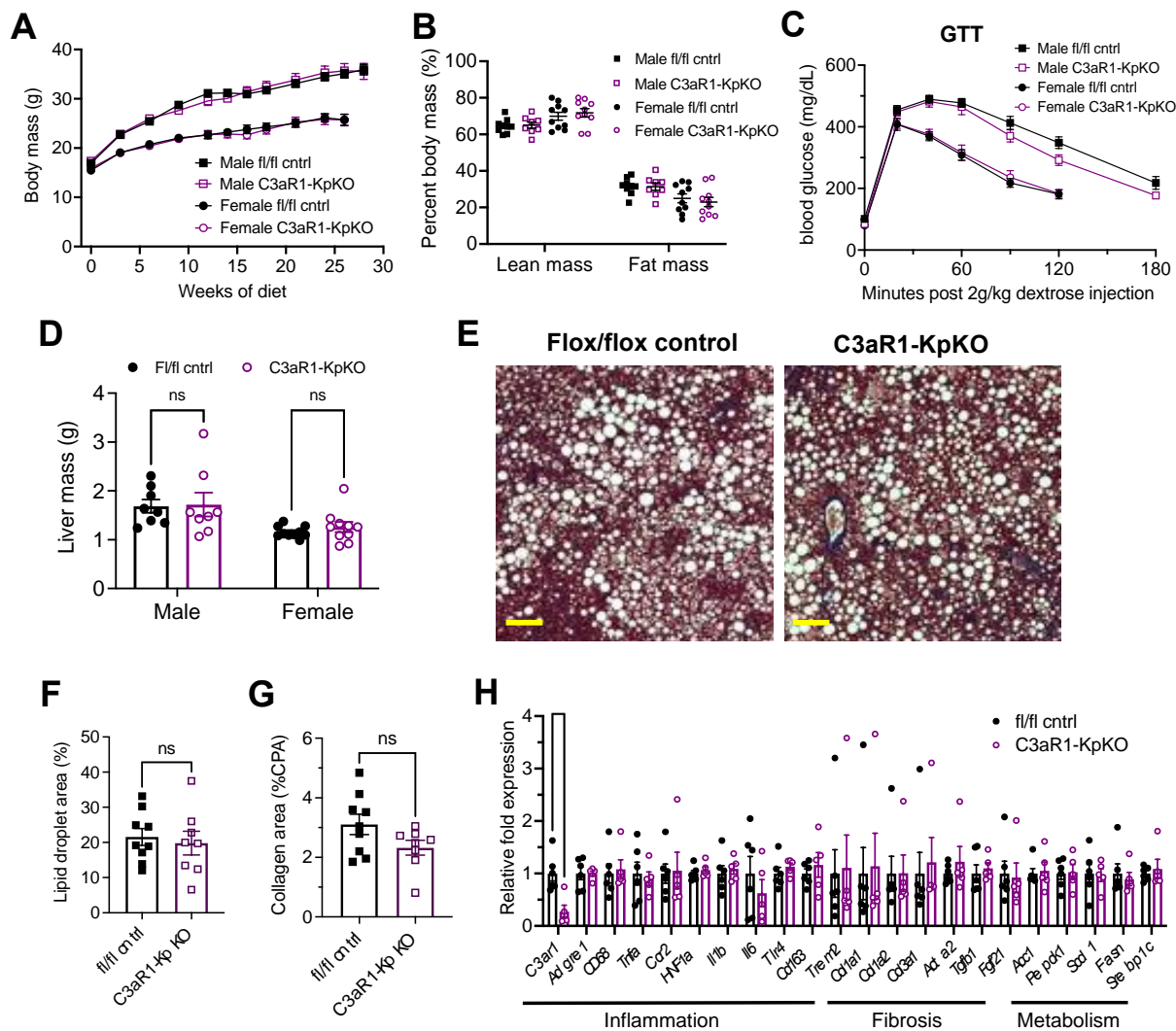
Figure 2. C3aR1 deletion in all macrophages does not affect weight gain, glucose homeostasis, liver steatosis or fibrosis.

- A) Expression of *C3ar1* in isolated peritoneal F4/80+/CD11b+ cells from floxed control mice (n = 6) or C3aR1-Mj KO male mice (n = 3).
- B) Expression of *C3ar1* in whole liver from control or C3aR1-Mj KO mice (n = 11-12 per male group, n = 13-14 per female group).
- C) Body mass curve of control or C3aR1-Mj KO mice on GAN high-fat diet starting at 5 weeks of age (n = 11-12 per male group, n = 14 per female group).
- D) Body composition analysis by EchoMRI in control or C3aR1-Mj KO mice after 30 weeks GAN diet (n = 6-9 per male group, n = 9-13 per female group).
- E) Glucose tolerance test in control or C3aR1-Mj KO mice with 14h fast after 28 weeks GAN diet (n = 6-9 per male group, n = 9-14 per female group).
- F) Liver mass in control or C3aR1-Mj KO male mice at time of euthanasia after 30 weeks GAN diet (n = 6-9 per male group, n = 9-14 per female group).
- G) Representative liver section staining by Masson's Trichrome in male control or C3aR1-Mj KO mice (scale bar = 100 μ m).
- H) Lipid droplet area in liver sections from male control or C3aR1-Mj KO mice, excluding vessel lumens (n = 6-7 per group).
- I) Collagen area in liver sections from male control or C3aR1-Mj KO mice (n = 6-7 per group).
- J) Relative fold expression of key gene markers for fibrosis, inflammation, and liver metabolism in whole liver from male control or C3aR1-Mj KO mice after 30 weeks GAN diet (n = 11-12 per group).
- Unpaired two-tailed Student's *t* test: Student's *t* test: *, p < 0.05.

368
369

370

Figure 3.



371
372

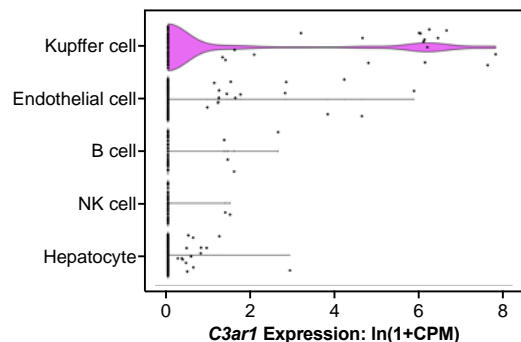
Figure 3. C3aR1 deletion in Kupffer cells does not affect weight gain, glucose homeostasis, liver steatosis or fibrosis.

- A) Body mass on GAN diet in flox/flox control or C3aR1-KpKO mice beginning at 5 weeks of age (n = 8-10 per group).
 B) Body composition analysis by EchoMRI in control or C3aR1-KpKO mice after 28 weeks GAN diet (n = 8-10).
 C) Glucose tolerance test in control or C3aR1-KpKO mice with 14h fast after 26 weeks GAN diet (n = 8-10).
 D) Liver mass in control or C3aR1-KpKO male mice at time of euthanasia after 28 weeks GAN diet (n = 8-10).
 E) Representative liver section staining by Masson's Trichrome in control or C3aR1-KpKO male mice (scale bar = 100 μ m).
 F) Lipid droplet area quantified on liver sections of control or C3aR1-KpKO male mice, excluding vessel lumens (n = 8-9).
 G) Collagen area quantified on whole liver section of control or C3aR1-KpKO male mice (n = 8-9).
 H) Relative gene expression in control or C3aR1-KpKO male mice after 30 weeks GAN diet (n = 5-6).
 Unpaired two-tailed Student's *t* test: **, p < 0.01.

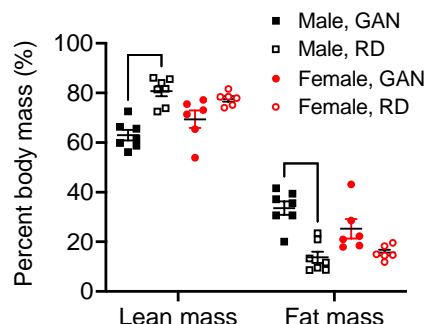
373

Supplementary Figures.

S1



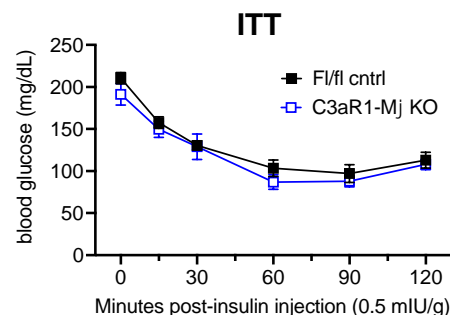
S2



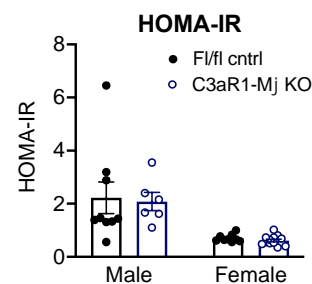
S3



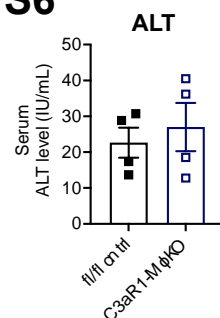
S4



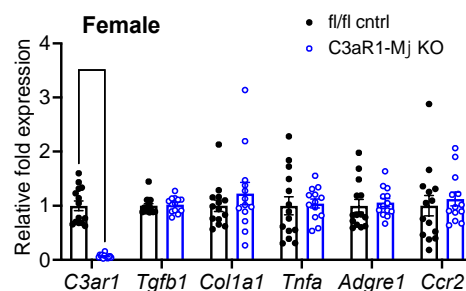
S5



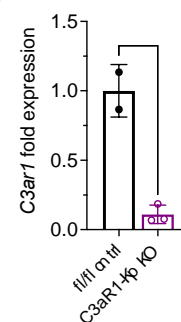
S6



S7



S8



374
375

Supplementary figures.

- S1) Single cell RNA sequencing analysis of *C3ar1* expression in mouse liver tissue (see text).
 S2) Percent lean and fat mass of flox/flox control mice after 20 weeks of GAN or RD diet (n = 6-7 per group).
 S3) Absolute lean and fat mass of flox/flox control mice after 20 weeks of GAN or RD diet (n = 6-7 per group).
 S4) Insulin tolerance test in control or C3aR1-Mj KO male mice with 14h fast after 29 weeks GAN diet (n = 6-9 per group).
 S5) HOMA-IR measurement of insulin resistance in control or C3aR1-Mj KO mice with 6h fast after 27 weeks GAN diet (n = 6-9 per male group, n = 9-13 per female group).
 S6) Serum alanine aminotransferase levels in control or C3aR1-Mj KO male mice after 30 weeks GAN diet (n = 4 per group).
 S7) Relative gene expression in control or C3aR1-Mj KO female mice after 30 weeks GAN diet (n = 13-14 per group).
 S8) Relative *C3ar1* expression in control or C3aR1-KpKO female mice after 30 weeks RD diet (n = 2-3 per group).
 Unpaired two-tailed Student's *t* test: **, $p < 0.01$; ***, $p < 0.001$.

376

377 **Supplementary Table S1.**

<i>Mus musculus</i> gene name	Forward qPCR primer	Reverse qPCR primer
Acc2	GCCTCCACTCACATTGGTTT	ATTGAAGAAAGCTGGGCTGA
Acta2	GGCTCTGGGCTCTGTAAGG	CTCTTGCTCTGGGCTTCATC
Adgre1	TGCATCTAGCAATGGACAGC	GCCTTCTGGATCCATTTGAA
C3ar1	TGACAGGTCAGCTCCTTCCT	CATTAGGAGGCTTTCCACCA
Ccr2	ATCCACGGCATACTATCAACATC	CAAGGCTCACCATCATCGTAG
Cd163	TCCACACGTCCAGAACAGTC	CCTTGAAACAGAGACAGGC
Cfd	CGTACCATGACGGGGTAGTC	ATCCGGTAGGATGACACTCG
Col1a1	GTGCTCCTGGTATTGCTGGT	GGCTCCTCGTTTTCTTCTT
Col1a2	GCCACCATTGATAGTCTCTCC	CACCCAGCGAAGAACTCATA
Col3a1	GGGTTTCCCTGGTCCTAAAG	CCTGGTTTCCCATTTTCTCC
Fasn	TTGCTGGCACTACAGAATGC	AACAGCCTCAGAGCGACAAT
Fgf21	CTGCTGGGGTCTACCAAG	CTGCGCTACCACTGTTCC
Hnf1a	GACCTGACCGAGTTGCCTAAT	CCGGCTCTTTCAGAATGGGT
Il1b	CTGGTGTGTGACGTTCCCATTA	CCGACAGCACGAGGCTTT
Il6	ACAACCACGGCCTTCCCTACTT	CACGATTTCCAGAGAACATGTG
Pepck1	TCATCATCACCCAAGAGCAG	CACATAGGGCGAGTCTGTCA
Rps18	CATGCAGAACCCACGACAGTA	CCTCACGCAGCTTGTTGTCTA
Scd1	CGCCCAAGCTGGAGTACGTC	CGCCCAAGCTGGAGTACGTC
Srebp1c	CTGGCAGTTCCATTGACAAG	ACTGAAGCTGGTGACTGCTG
Tgfb1	TGCGCTTGCAGAGATTAATA	AGCCCTGTATTCCGTCTCCT
Tlr4	TGTCATCAGGGACTTTGCTG	GGACTCTGATCATGGCACTG
Tnfa	ACGGCATGGATCTCAAAGAC	AGATAGCAAATCGGCTGACG
Trem2	CTACCAGTGTCAGAGTCTCCGA	CCTCGAAACTCGATGACTCCTC

379 **References**

- 380 1 Ge, X., Zheng, L., Wang, M., Du, Y. & Jiang, J. Prevalence trends in non-alcoholic fatty
381 liver disease at the global, regional and national levels, 1990-2017: a population-based
382 observational study. *BMJ Open* **10**, e036663 (2020). [https://doi.org/10.1136/bmjopen-](https://doi.org/10.1136/bmjopen-2019-036663)
383 [2019-036663](https://doi.org/10.1136/bmjopen-2019-036663)
- 384 2 Younossi, Z. *et al.* Global burden of NAFLD and NASH: trends, predictions, risk factors
385 and prevention. *Nat Rev Gastroenterol Hepatol* **15**, 11-20 (2018).
386 <https://doi.org/10.1038/nrgastro.2017.109>
- 387 3 Ferguson, D. & Finck, B. N. Emerging therapeutic approaches for the treatment of
388 NAFLD and type 2 diabetes mellitus. *Nat Rev Endocrinol* **17**, 484-495 (2021).
389 <https://doi.org/10.1038/s41574-021-00507-z>
- 390 4 Friedman, S. L., Neuschwander-Tetri, B. A., Rinella, M. & Sanyal, A. J. Mechanisms of
391 NAFLD development and therapeutic strategies. *Nat Med* **24**, 908-922 (2018).
392 <https://doi.org/10.1038/s41591-018-0104-9>
- 393 5 Stefan, N., Haring, H. U. & Cusi, K. Non-alcoholic fatty liver disease: causes, diagnosis,
394 cardiometabolic consequences, and treatment strategies. *Lancet Diabetes Endocrinol* **7**,
395 313-324 (2019). [https://doi.org/10.1016/S2213-8587\(18\)30154-2](https://doi.org/10.1016/S2213-8587(18)30154-2)
- 396 6 Kim, H. *et al.* Metabolic Spectrum of Liver Failure in Type 2 Diabetes and Obesity: From
397 NAFLD to NASH to HCC. *Int J Mol Sci* **22** (2021). <https://doi.org/10.3390/ijms22094495>
- 398 7 Duell, P. B. *et al.* Nonalcoholic Fatty Liver Disease and Cardiovascular Risk: A Scientific
399 Statement From the American Heart Association. *Arterioscler Thromb Vasc Biol* **42**,
400 e168-e185 (2022). <https://doi.org/10.1161/ATV.000000000000153>
- 401 8 Kasper, P. *et al.* NAFLD and cardiovascular diseases: a clinical review. *Clin Res Cardiol*
402 **110**, 921-937 (2021). <https://doi.org/10.1007/s00392-020-01709-7>
- 403 9 Barreby, E., Chen, P. & Aouadi, M. Macrophage functional diversity in NAFLD - more
404 than inflammation. *Nat Rev Endocrinol* **18**, 461-472 (2022).
405 <https://doi.org/10.1038/s41574-022-00675-6>
- 406 10 Cai, J., Zhang, X. J. & Li, H. The Role of Innate Immune Cells in Nonalcoholic
407 Steatohepatitis. *Hepatology* **70**, 1026-1037 (2019). <https://doi.org/10.1002/hep.30506>
- 408 11 Guilliams, M. & Scott, C. L. Liver macrophages in health and disease. *Immunity* **55**,
409 1515-1529 (2022). <https://doi.org/10.1016/j.immuni.2022.08.002>
- 410 12 Park, S. J., Garcia Diaz, J., Um, E. & Hahn, Y. S. Major roles of kupffer cells and
411 macrophages in NAFLD development. *Front Endocrinol (Lausanne)* **14**, 1150118 (2023).
412 <https://doi.org/10.3389/fendo.2023.1150118>
- 413 13 Sakai, M. *et al.* Liver-Derived Signals Sequentially Reprogram Myeloid Enhancers to
414 Initiate and Maintain Kupffer Cell Identity. *Immunity* **51**, 655-670 e658 (2019).
415 <https://doi.org/10.1016/j.immuni.2019.09.002>
- 416 14 Krenkel, O. *et al.* Myeloid cells in liver and bone marrow acquire a functionally distinct
417 inflammatory phenotype during obesity-related steatohepatitis. *Gut* **69**, 551-563 (2020).
418 <https://doi.org/10.1136/gutjnl-2019-318382>
- 419 15 Guilliams, M. *et al.* Spatial proteogenomics reveals distinct and evolutionarily conserved
420 hepatic macrophage niches. *Cell* **185**, 379-396 e338 (2022).
421 <https://doi.org/10.1016/j.cell.2021.12.018>
- 422 16 Govaere, O. *et al.* Transcriptomic profiling across the nonalcoholic fatty liver disease
423 spectrum reveals gene signatures for steatohepatitis and fibrosis. *Sci Transl Med* **12**
424 (2020). <https://doi.org/10.1126/scitranslmed.aba4448>
- 425 17 Merle, N. S., Church, S. E., Fremeaux-Bacchi, V. & Roumenina, L. T. Complement
426 System Part I - Molecular Mechanisms of Activation and Regulation. *Front Immunol* **6**,
427 262 (2015). <https://doi.org/10.3389/fimmu.2015.00262>

- 428 18 Kolev, M. & Kemper, C. Keeping It All Going-Complement Meets Metabolism. *Front Immunol* **8**, 1 (2017). <https://doi.org/10.3389/fimmu.2017.00001>
- 429
- 430 19 Zhao, J. *et al.* Association of complement components with the risk and severity of
- 431 NAFLD: A systematic review and meta-analysis. *Front Immunol* **13**, 1054159 (2022).
- 432 <https://doi.org/10.3389/fimmu.2022.1054159>
- 433 20 Segers, F. M. *et al.* Complement alternative pathway activation in human nonalcoholic
- 434 steatohepatitis. *PLoS One* **9**, e110053 (2014).
- 435 <https://doi.org/10.1371/journal.pone.0110053>
- 436 21 Markiewski, M. M. & Lambris, J. D. The role of complement in inflammatory diseases
- 437 from behind the scenes into the spotlight. *Am J Pathol* **171**, 715-727 (2007).
- 438 <https://doi.org/10.2353/ajpath.2007.070166>
- 439 22 Yadav, M. K. *et al.* Molecular basis of anaphylatoxin binding, activation, and signaling
- 440 bias at complement receptors. *Cell* **186**, 4956-4973 e4921 (2023).
- 441 <https://doi.org/10.1016/j.cell.2023.09.020>
- 442 23 Flier, J. S., Cook, K. S., Usher, P. & Spiegelman, B. M. Severely impaired adiponin
- 443 expression in genetic and acquired obesity. *Science* **237**, 405-408 (1987).
- 444 <https://doi.org/10.1126/science.3299706>
- 445 24 Xu, Y. *et al.* Complement activation in factor D-deficient mice. *Proc Natl Acad Sci U S A*
- 446 **98**, 14577-14582 (2001). <https://doi.org/10.1073/pnas.261428398>
- 447 25 Lim, J. *et al.* C5aR and C3aR antagonists each inhibit diet-induced obesity, metabolic
- 448 dysfunction, and adipocyte and macrophage signaling. *FASEB J* **27**, 822-831 (2013).
- 449 <https://doi.org/10.1096/fj.12-220582>
- 450 26 Polyzos, S. A., Kountouras, J. & Mantzoros, C. S. Adipokines in nonalcoholic fatty liver
- 451 disease. *Metabolism* **65**, 1062-1079 (2016).
- 452 <https://doi.org/10.1016/j.metabol.2015.11.006>
- 453 27 Han, J. & Zhang, X. Complement Component C3: A Novel Biomarker Participating in the
- 454 Pathogenesis of Non-alcoholic Fatty Liver Disease. *Front Med (Lausanne)* **8**, 653293
- 455 (2021). <https://doi.org/10.3389/fmed.2021.653293>
- 456 28 Lo, J. C. *et al.* Adiponin is an adipokine that improves beta cell function in diabetes. *Cell*
- 457 **158**, 41-53 (2014). <https://doi.org/10.1016/j.cell.2014.06.005>
- 458 29 Gomez-Banoy, N. *et al.* Adiponin preserves beta cells in diabetic mice and associates with
- 459 protection from type 2 diabetes in humans. *Nat Med* **25**, 1739-1747 (2019).
- 460 <https://doi.org/10.1038/s41591-019-0610-4>
- 461 30 Mamane, Y. *et al.* The C3a anaphylatoxin receptor is a key mediator of insulin resistance
- 462 and functions by modulating adipose tissue macrophage infiltration and activation.
- 463 *Diabetes* **58**, 2006-2017 (2009). <https://doi.org/10.2337/db09-0323>
- 464 31 Han, J. *et al.* Bone marrow-derived macrophage contributes to fibrosing steatohepatitis
- 465 through activating hepatic stellate cells. *J Pathol* **248**, 488-500 (2019).
- 466 <https://doi.org/10.1002/path.5275>
- 467 32 Boland, M. L. *et al.* Towards a standard diet-induced and biopsy-confirmed mouse model
- 468 of non-alcoholic steatohepatitis: Impact of dietary fat source. *World J Gastroenterol* **25**,
- 469 4904-4920 (2019). <https://doi.org/10.3748/wjg.v25.i33.4904>
- 470 33 Hansen, H. H. *et al.* Human translatability of the GAN diet-induced obese mouse model
- 471 of non-alcoholic steatohepatitis. *BMC Gastroenterol* **20**, 210 (2020).
- 472 <https://doi.org/10.1186/s12876-020-01356-2>
- 473 34 Vacca, M. *et al.* An unbiased ranking of murine dietary models based on their proximity
- 474 to human metabolic dysfunction-associated steatotic liver disease (MASLD). *Nat Metab*
- 475 (2024). <https://doi.org/10.1038/s42255-024-01043-6>
- 476 35 Uhlen, M. *et al.* Proteomics. Tissue-based map of the human proteome. *Science* **347**,
- 477 1260419 (2015). <https://doi.org/10.1126/science.1260419>

- 478 36 MacParland, S. A. *et al.* Single cell RNA sequencing of human liver reveals distinct
479 intrahepatic macrophage populations. *Nat Commun* **9**, 4383 (2018).
480 [https://doi.org:10.1038/s41467-018-06318-7](https://doi.org/10.1038/s41467-018-06318-7)
- 481 37 Tabula Muris, C. *et al.* Single-cell transcriptomics of 20 mouse organs creates a Tabula
482 Muris. *Nature* **562**, 367-372 (2018). [https://doi.org:10.1038/s41586-018-0590-4](https://doi.org/10.1038/s41586-018-0590-4)
- 483 38 Suppli, M. P. *et al.* Hepatic transcriptome signatures in patients with varying degrees of
484 nonalcoholic fatty liver disease compared with healthy normal-weight individuals. *Am J*
485 *Physiol Gastrointest Liver Physiol* **316**, G462-G472 (2019).
486 [https://doi.org:10.1152/ajpgi.00358.2018](https://doi.org/10.1152/ajpgi.00358.2018)
- 487 39 Ma, L. *et al.* Adipsin and Adipocyte-derived C3aR1 Regulate Thermogenic Fat in a Sex-
488 dependent Fashion. *JCI Insight* (2024). [https://doi.org:10.1172/jci.insight.178925](https://doi.org/10.1172/jci.insight.178925)
- 489 40 Kong, L. R. *et al.* Loss of C3a and C5a receptors promotes adipocyte browning and
490 attenuates diet-induced obesity via activating inosine/A2aR pathway. *Cell Rep* **42**,
491 112078 (2023). [https://doi.org:10.1016/j.celrep.2023.112078](https://doi.org/10.1016/j.celrep.2023.112078)
- 492 41 Li, X. *et al.* A new NASH model in aged mice with rapid progression of steatohepatitis
493 and fibrosis. *PLoS One* **18**, e0286257 (2023).
494 [https://doi.org:10.1371/journal.pone.0286257](https://doi.org/10.1371/journal.pone.0286257)
- 495 42 Cumpelik, A. *et al.* Dynamic regulation of B cell complement signaling is integral to
496 germinal center responses. *Nat Immunol* **22**, 757-768 (2021).
497 [https://doi.org:10.1038/s41590-021-00926-0](https://doi.org/10.1038/s41590-021-00926-0)
- 498 43 Zhang, X., Goncalves, R. & Mosser, D. M. The isolation and characterization of murine
499 macrophages. *Curr Protoc Immunol* **Chapter 14**, 14 11 11-14 11 14 (2008).
500 [https://doi.org:10.1002/0471142735.im1401s83](https://doi.org/10.1002/0471142735.im1401s83)
501